ACS APPLIED MATERIALS & INTERFACES

www.acsami.org

Research Article

Photothermal Shape-Memory Nanofibrous Membrane for Efficient Recovery of High-Viscosity Crude Oil

Qiong Zuo,[§] Lingyu Zhao,*[,§] Qingyuan Du, Zengbai Ouyang, Yutong Wang, Dazhi Sun, and Jinsong Leng*

Cite This: https://doi.org/10.1021/acsami.6c03950

Read Online

ACCESS | Metrics & More | Article Recommendations | Supporting Information

ABSTRACT: Efficient recovery of highly viscous crude oil remains a critical challenge due to the poor mobility and slow diffusion of such oils under ambient conditions. Here, a photothermal shape-memory nanofibrous membrane (CB@AUA/SIS) was developed via the electrospinning of aliphatic polyurethane acrylate (AUA) and polystyrene-*block*-polyisoprene-*block*-polystyrene (SIS), incorporating carbon black (CB) as a low-cost photothermal filler. The electrospun architecture provides a high surface area and porosity, while the CB endows the membrane with light absorption (reaching 98%) and a high photothermal conversion efficiency of 73.4%. Upon irradiation, the membrane rapidly heats to 61.2 °C, effectively reducing the viscosity of crude oil. Together with the intrinsic lipophilicity of the AUA/SIS copolymer, a high adsorption rate of 6240 $g \cdot m^{-2} \cdot min^{-1}$ is achieved. In addition, the membrane exhibits excellent hydrophobicity and a light-responsive shape memory effect. This allows the folded structure to autonomously unfold on water surfaces, facilitating its intelligent deployment. Outdoor sunlight tests further confirm its reliable performance. This work demonstrates a multifunctional, light-adaptive system that integrates solar-driven heating and programmable shape transformation for the remediation of viscous crude oil spills.

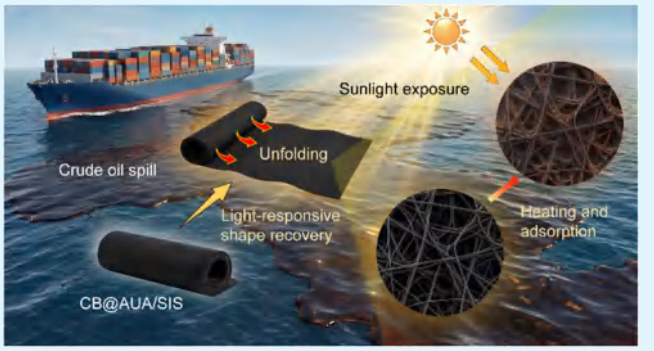

KEYWORDS: *electrospinning, nanofibrous membrane, photothermal conversion, shape memory effect, light-responsive, crude oil adsorption*

INTRODUCTION

Crude oil stands as one of the most important global energy resources, yet accidental leakage during extraction, transportation, and storage remains a persistent risk.[1−3] Such spills pose severe threats to aquatic ecosystems and human health, highlighting the urgent demand for efficient adsorbent materials for oil−water remediation.[4−6] Conventional porous adsorbents, such as polyurethane foams,[7,8] melamine sponges,[9,10] and aerogels,[11,12] have been widely explored owing to their low density and high porosity. Nevertheless, while these materials exhibit efficient adsorption toward light oils with low viscosity (<100 mPa·s),[13,14] their capacity is severely compromised when exposed to highly viscous crude oils. This is primarily due to the limited fluidity and sluggish diffusion of the latter,[15,16] which significantly restricts their practical applicability in tackling high-viscosity crude oil spills.

To overcome these limitations, photothermal conversion materials have recently garnered increasing attention.[17−20] By harvesting solar energy and converting it into heat, these materials can effectively lower oil viscosity and promote the penetration of oil into porous structures, thereby enhancing the adsorption efficiency.[21] Various photothermal agents, including carbon nanomaterials,[10] MXene nanosheets,[22] conductive polymers,[23] and metal oxides,[24] have been incorporated into porous matrices to enhance light absorption. These systems have shown improved performance in crude oil remediation. However, conventional adsorbents face challenges in transport and deployment, as their bulky structures hinder efficient storage and operation.[25] This highlights the need for adsorbents that combine high efficiency with improved portability.

Electrospinning provides a facile strategy for constructing fibrous membranes with high specific surface area and porosity, enabling efficient oil capture and functional modification.[26−28] This technique allows incorporation of functional fillers, such as photothermal agents, without compromising the membrane's structural integrity.[29,30] The development of stimuli-responsive smart materials, particularly shape memory polymers that can recover their original geometry upon exposure to specific triggers, offers a promising strategy to enhance material applicability.[31−34] Incorporating shape

Received: February 25, 2026
Revised: June 1, 2026
Accepted: June 1, 2026

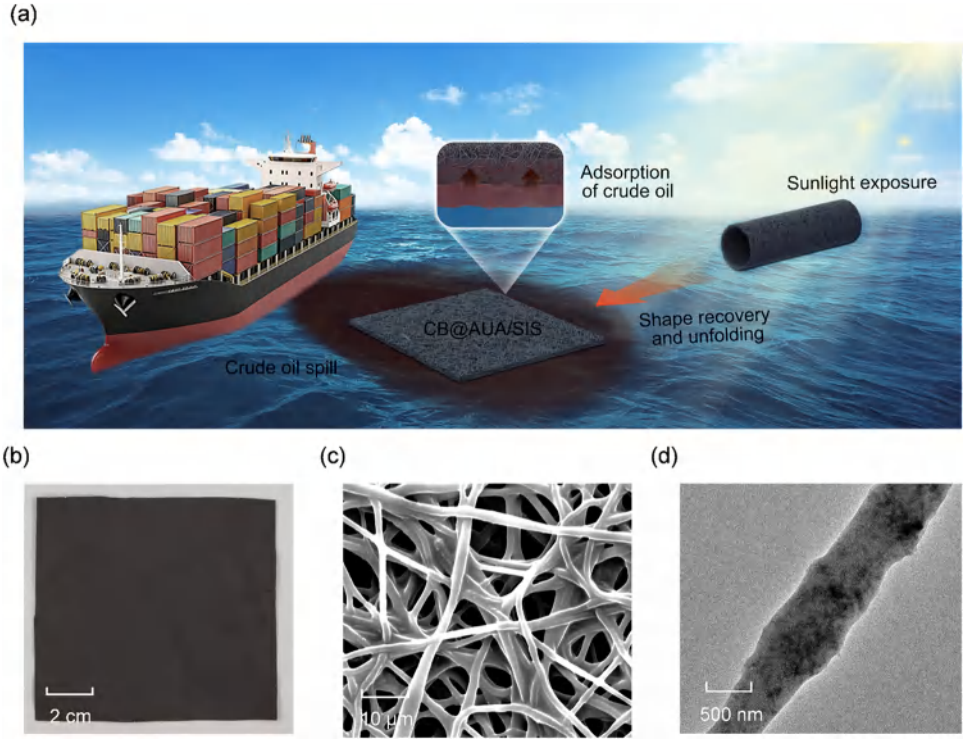

Figure 1. The design and preparation of the CB@AUA/SIS membrane. (a) Diagram of the solar-powered and self-heating SMP for crude oil adsorption. (b) Photograph of a 10 × 10 cm^2 CB@AUA/SIS membrane. (c) SEM image of the fibrous network, and (d) TEM image of a CB@AUA/SIS fiber.

memory behavior into electrospun fibers enables the material to be folded for transport. And it allows the membrane to autonomously unfold for operation, ensuring both convenience and high performance in oil adsorption.

Herein, we report an electrospun nanofibrous composite membrane composed of aliphatic polyurethane acrylate (AUA) and polystyrene-*block*-polyisoprene-*block*-polystyrene (SIS), incorporating carbon black (CB) as a cost-effective photothermal filler. The electrospun architecture provides a high specific surface area and mechanical robustness, while the embedded CB ensures efficient solar energy conversion, with a photothermal conversion efficiency of 73.4% and a broadband light absorption of up to 98%. Under 1 sun irradiation, the membrane can be rapidly heated to 61.2 °C, which effectively reduces the viscosity of crude oil and promotes a spontaneous adsorption process. Besides, the AUA/SIS copolymer's intrinsic lipophilicity further facilitates the entry of oil into the film. Thus, a high adsorption rate of 6240 $g{\cdot}m^{-2}{\cdot}min^{-1}$ was achieved. In addition, the composite exhibits excellent hydrophobicity and oleophilicity, enabling the selective removal of floating crude oil. The membrane features a light-responsive shape memory effect that enables self-unfolding on the water surface and recovery of its original structure after folding or deformation, facilitating transportation, deployment, and ensuring stable oil adsorption performance under practical conditions.

RESULTS AND DISCUSSION

Design of CB@AUA/SIS

The working principle of the CB@AUA/SIS is shown in Figure 1a, highlighting the integration of light-responsive shape recovery and oil adsorption. The CB@AUA/SIS membrane was fabricated by electrospinning a blended precursor of AUA and SIS, followed by in situ UV curing. The strategy forms a copolymerized network with shape memory property, in which the AUA domains and cross-linking points serve as the fixed phase, while the soft segment of SIS acts as the reversible phase. This structure enables the membrane to recover its original shape in response to thermal stimuli.[35] In addition, the hydrocarbon-rich segments of SIS impart strong oleophilicity, which favors selective oil uptake. As a low-cost and efficient photothermal agent, CB can rapidly harvest solar light to generate heat, thereby triggering the shape memory effect.[36] This design synergistically integrates photothermal responsiveness with shape memory behavior, enabling autonomous unfolding on the water surface and efficient recovery of viscous crude oil. Large-area membranes with dimensions up to 10 × 10 cm^2 were fabricated (Figure 1b), exhibiting uniform surfaces that confirm the feasibility of scalable fabrication. Figure 1c presents the morphology of the electrospun membrane, revealing a continuous fibrous network with interconnected pores.[37] A structural comparison with the AUA/SIS membrane demonstrates that CB incorporation optimizes the pore parameters (Figure S1). The porosity increased from 28.4% to 50.3%, and the total pore area expanded from 1.948 m^2/g to 14.882 m^2/g. Furthermore, an increase in pore diameter was observed following CB doping. The high porosity and large pore area of this network provide ample storage capacity and abundant interfaces, which are conducive to rapid oil infiltration and storage. The TEM image shows that the CB fillers (black regions within the fiber) are rather uniformly dispersed along the fiber surface and are anchored to the fiber matrix, rather than aggregating within the pores (Figure 1d). This configuration ensures effective contact between the conductive fillers and the polymer while

https://doi.org/10.1021/acsami.6c03950
ACS Appl. Mater. Interfaces XXXX, XXX, XXX−XXX

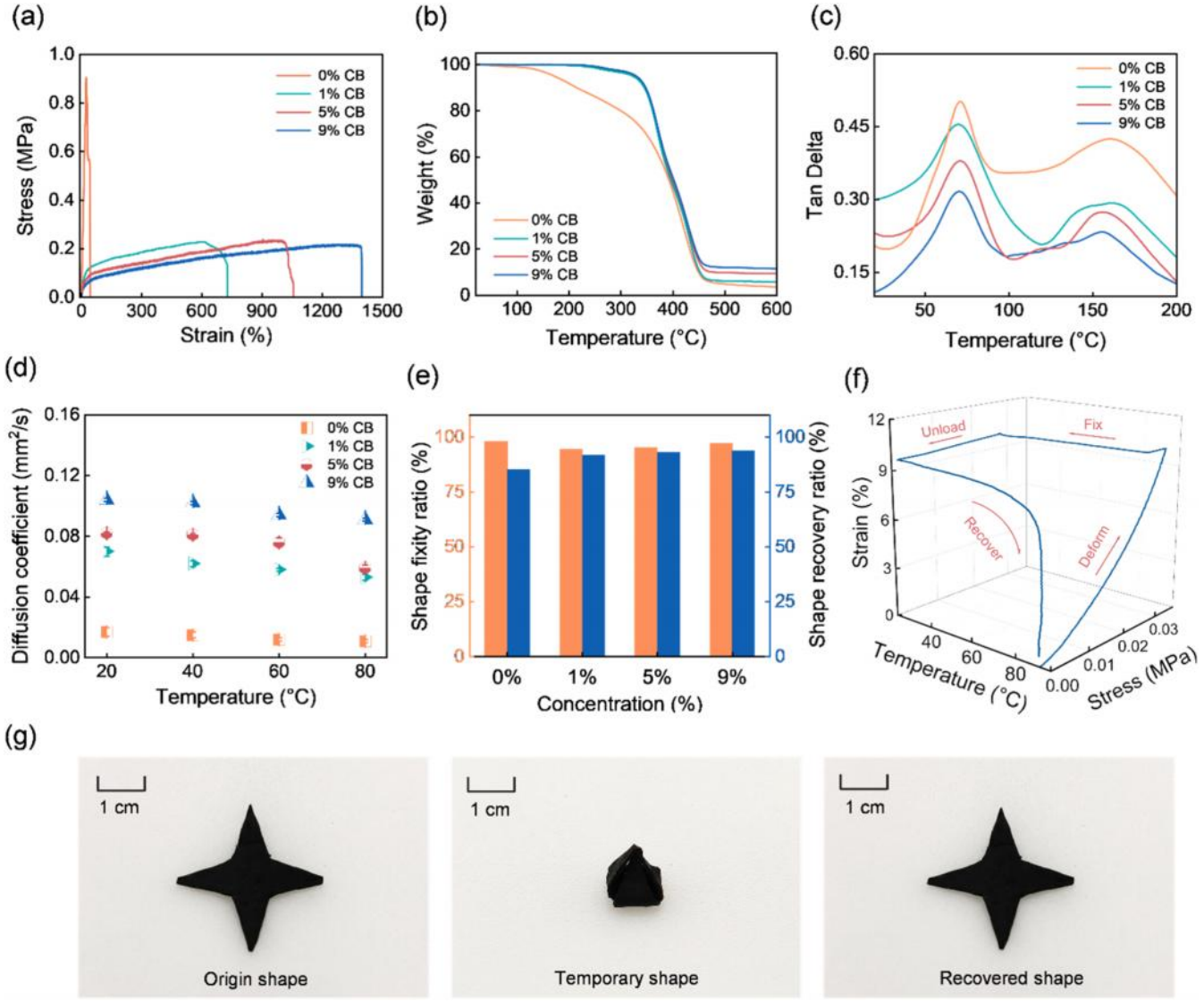

Figure 2. The properties of the CB@AUA/SIS membrane. (a) Stress−strain curves, (b) TGA, (c) Tan Delta, (d) Thermal diffusivity, and (e) Shape fixity and recovery performance of AUA/SIS and CB@AUA/SIS membrane. (f) 3D diagram of the shape memory cycle of the CB@AUA/SIS membrane. (g) Photographs of the shape memory behavior of CB@AUA/SIS upon heating.

minimizing particle detachment during operation. The successful integration of CB into the fibrous network is further supported by energy dispersive spectroscopy (EDS), which shows a marked increase in carbon content (Figure S2).

The Selection of Fillers for CB@AUA/SIS

The CB content within the CB@AUA/SIS was optimized to achieve a balanced structure and functionality. Membranes with CB contents of 0, 1, 5, and 9 wt % were prepared at the AUA/SIS ratio of 1:2. When the CB content exceeded 9 wt %, premature curing occurred during electrospinning, leading to unstable jets and nonuniform membranes. Fibers containing 13 wt % CB exhibited irregular morphology and poor uniformity, confirming the adverse effect of excessive filler incorporation on processability (Figure S3). Therefore, the membrane with 13% CB was excluded from the following comparisons. As shown in Figure 2a, the incorporation of CB affected the mechanical properties of the membranes. The elongation at break increased with CB content, while the storage modulus decreased (Figure S4), indicating that higher filler content made the membranes more elastic and deformable. The enhanced elasticity enables greater strain during the shape programming, providing improved flexibility for deformation. The thermal stability of the polymer matrix also improved at higher CB concentrations (Figure 2b). Tan Delta curves revealed two distinct peaks, corresponding to the segmental relaxations of the SIS and AUA domains (Figure 2c). The low-temperature peak reflects the glass transition of the SIS-rich soft segments, which is closely related to the shape recovery process and serves as the switching temperature (T_w) of the composite. Upon CB incorporation, this low-temperature peak shifted, indicative of enhanced chain mobility. The high-temperature transition remained unchanged, indicating preserved hard-phase integrity.[38,39] The thermal diffusivity increased with CB loading (Figure 2d), reflecting improved heat transfer capability imparted by the carbonaceous filler. These characteristics provide favorable conditions for the shape memory process.

As shown in Figure 2e, the 9 wt % CB@AUA/SIS exhibited the highest shape recovery efficiency. This enhancement originates from the dual contributions of CB: enhancing

https://doi.org/10.1021/acsami.6c03950
ACS Appl. Mater. Interfaces XXXX, XXX, XXX−XXX

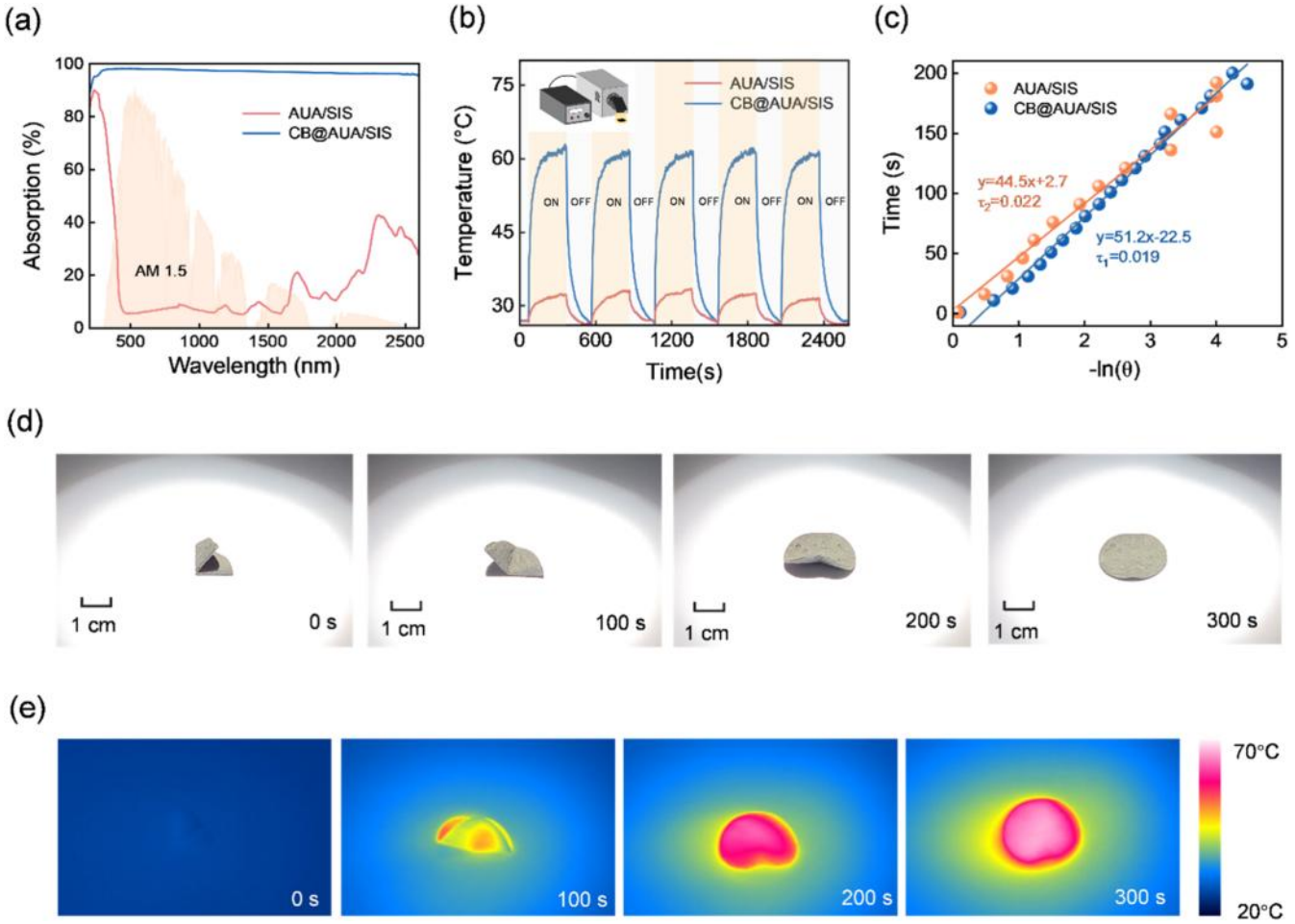

Figure 3. Photothermal performance of CB@AUA/SIS membrane. (a) UV−Vis-NIR absorption spectra of the AUA/SIS and CB@AUA/SIS membrane. (b) Surface temperature variations of AUA/SIS and CB@AUA/SIS membrane for 5 light on/off cycles. (c) Measurement of the sample system time constant at 1 kW·m^{-2}. (d) Photographs and (e) The thermal images of the CB@AUA/SIS membrane under the light-responsive shape recovery process.

thermal conductivity to enable faster heating, while simultaneously weakening intermolecular interactions within the polymer matrix, thereby facilitating soft segment motion during recovery.[40] From the representative shape memory diagram (Figure 2f), the CB@AUA/SIS shows a typical thermal shape memory behavior, with a strain fixity ratio (R_f) of 97.3% and a strain recovery ratio (R_r) of 94%, respectively. The reliable shape recovery behavior was also confirmed by visual evidence in which a severely folded star-shaped membrane completely returns to the original shape upon 40 s of heating (Figure 2g). Therefore, considering the excellent shape recovery efficiency and balanced thermomechanical properties, the 9 wt % CB@AUA/SIS membrane was selected for this study. Subsequent experiments evaluated the photothermal heating and oil adsorption performances of the membranes with different CB contents (1, 5, and 9 wt %). Under identical irradiation conditions, the 9 wt % membrane achieved efficient temperature elevation (Figure S5) and the optimal oil adsorption capacity (Figure S6). These results corroborate the selection of this concentration for solar-driven viscous crude oil recovery.

Photothermal Effect of CB@AUA/SIS

CB@AUA/SIS membrane exhibited excellent photothermal performance and light-responsive shape memory behavior. It has strong broadband absorption, achieving a peak absorption of 98% across the UV−vis−NIR region (Figure 3a), which enabled efficient light-to-heat conversion. Upon exposure to 1 kW·m^{-2} irradiation (1 sun), the CB@AUA/SIS membrane rapidly heated to 61.2 °C, whereas the AUA/SIS membrane exhibited a negligible temperature rise (Figure 3b). This rapid heating was confirmed by the infrared thermal images in Figure S7. Besides, the cycling curve of CB@AUA/SIS remained almost unchanged after five cycles of repeated temperature rises and falls, demonstrating the superior stability of its photothermal conversion efficiency. The photothermal conversion efficiency (η) was determined using an energy balance model. Based on the linear fitting of the cooling curve (Figure 3c), the η was calculated to be 73.4%.[18,41] The details are shown in the Experimental sections. The high efficiency confirms the effective utilization of solar energy, highlighting the role of CB incorporation in both enhancing light absorption and promoting efficient thermal energy conversion. The photothermal effect of CB@AUA/SIS can trigger its shape memory behavior under light irradiation. When the membrane temperature exceeded the transition temperature, the temporary shape recovered to its original shape. Sequential photographs and the video clearly show that complete shape recovery was achieved within 300 s (Figure 3d and Movie S1), with efficient heat diffusion across the entire film (Figure 3e).

https://doi.org/10.1021/acsami.6c03950
ACS Appl. Mater. Interfaces XXXX, XXX, XXX−XXX

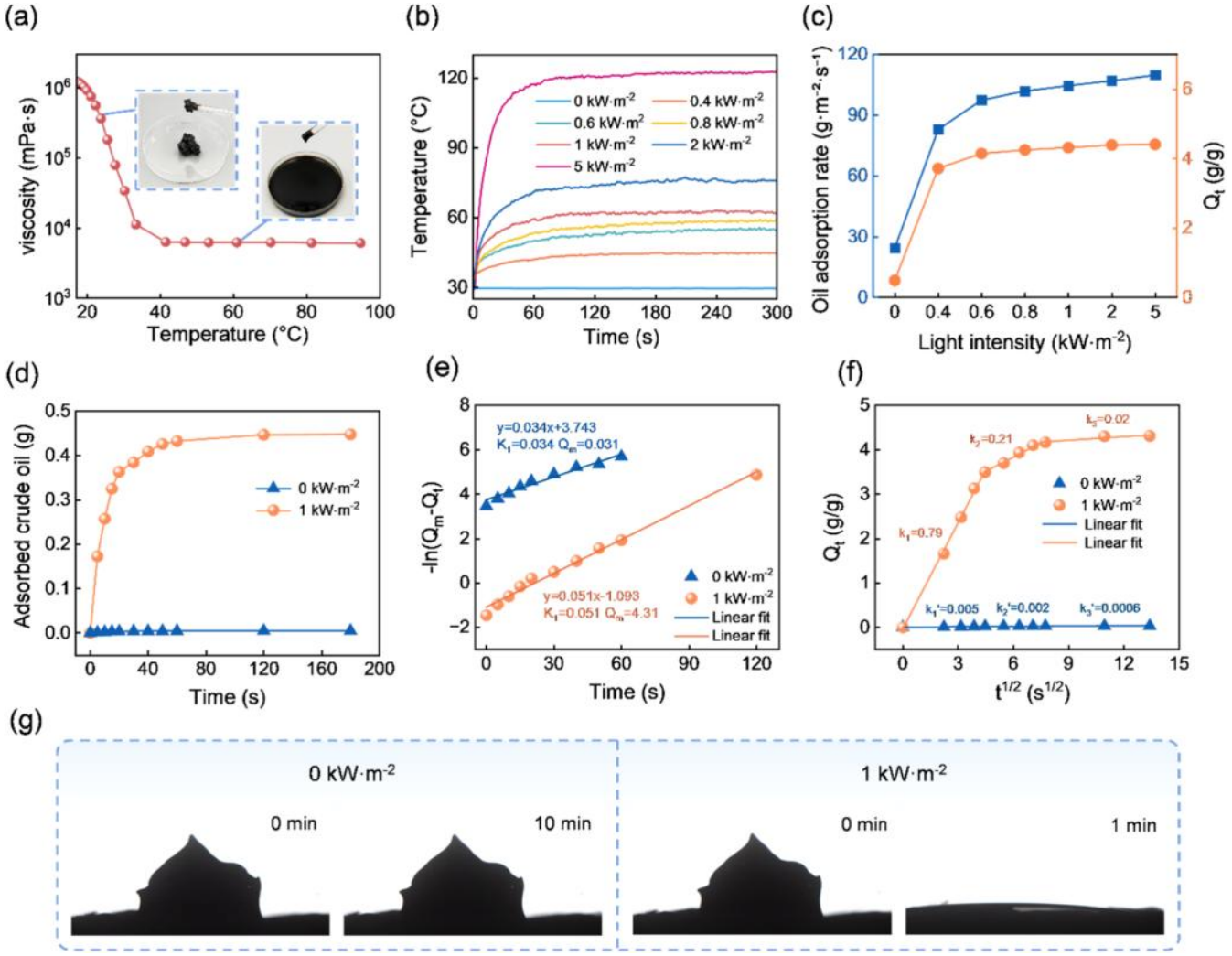

Figure 4. Crude oil adsorption capacity of the CB@AUA/SIS membrane (a) Crude oil viscosity under different temperatures. (b) Temperature–time curves and (c) Crude oil adsorption capacity of CB@AUA/SIS membrane under different light intensities. (d) Time-dependent oil adsorption capacity for the CB@AUA/SIS membrane. (e) Linear fit of the pseudo-first-order model and (f) Intraparticle diffusion model for the oil adsorption at 0 kW·m^{-2} and 1 kW·m^{-2}. (g) Images comparing the crude oil adsorption behavior under dark and illuminated conditions.

This process is consistent with thermally induced recovery, as the shape memory behavior in both cases is activated upon reaching the T_w obtained from the DMA results.

The Photothermal Effect of CB@AUA/SIS

The photothermal effect of CB@AUA/SIS membrane effectively enhances the adsorption of highly viscous crude oil. The oil used in this study exhibits a viscosity of 1.8×10^5 mPa·s at room temperature, which decreases rapidly with rising temperature (Figure 4a), indicating that external heating can effectively reduce viscosity and accelerate oil adsorption.[23] At an irradiation intensity of 1 kW·m^{-2}, the surface temperature exceeds 60 °C (Figure 4b), lowering oil viscosity to promote diffusion into the porous network. When the light intensity increases to 5 kW·m^{-2}, the surface temperature rises to 122 °C, demonstrating the excellent photothermal conversion capability of the material. Both the adsorption rate and capacity increased with higher light intensity (Figure 4c). At 1 kW·m^{-2}, the adsorption rate reaches 6240 g·m^{-2}·min^{-1}, markedly exceeding performance in the dark. The time-dependent adsorption curve also highlights this enhancement (Figure 4d). In the absence of light, there's almost no effective uptake of oil (0.004 g) throughout the process. In contrast, under 1 kW·m^{-2} irradiation, the adsorbed oil mass increased steadily with time and reached 0.45 g after ∼80 s, which clearly evidence the promotional effect of light irradiation. To analyze the adsorption mechanism, the data were fitted using the pseudo-first-order model described by eq 1[42]

$$\ln(Q_m - Q_t) = \ln(Q_m) - tk_1 \quad (1)$$

where Q_t represents the adsorption mass at the given time (g·g^{-1}), t is time (s), and k_1 is the adsorption rate constant (s^{-1}). This model describes the relationship between adsorption rate and time, allowing for the evaluation of Q_m and k_1. Fitting results revealed that the rate constant under irradiation (k_1 = 0.051, R^2 = 0.993) was higher than that in the dark (k_1 = 0.034), indicating a significantly accelerated adsorption rate under irradiation. The diffusion behavior of crude oil molecules within the porous network was analyzed using the intraparticle diffusion model shown in eq 2[43]

$$Q_t = kt^{1/2} + C \quad (2)$$

https://doi.org/10.1021/acsami.6c03950
ACS Appl. Mater. Interfaces XXXX, XXX, XXX−XXX

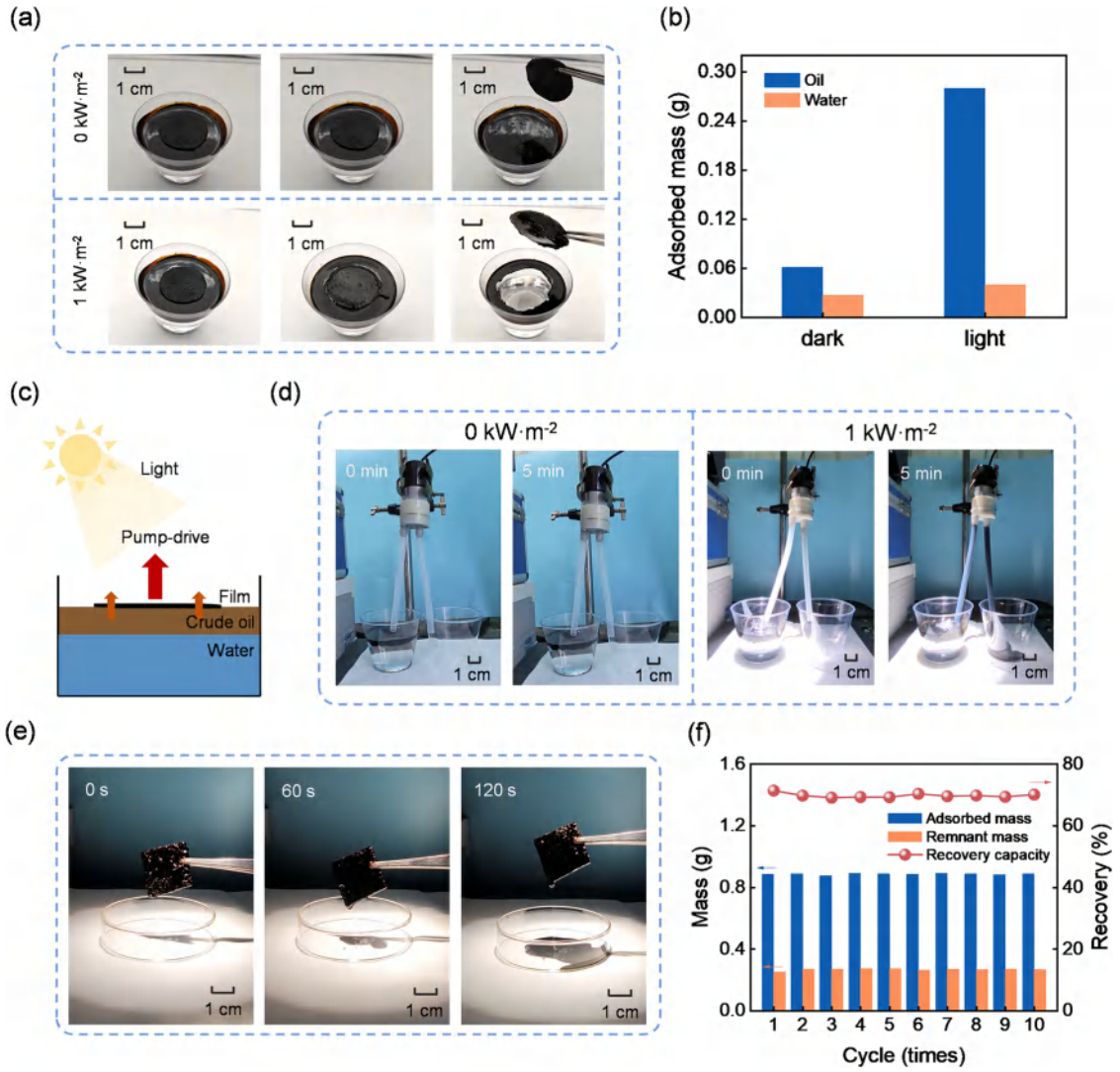

Figure 5. The application of the CB@AUA/SIS membrane under light irradiation. (a) Photograph of CB@AUA/SIS adsorbing oil on the water surface and (b) The amount of adsorbed crude oil and water under light illumination and dark conditions. (c) The schematic of floating oil collection using CB@AUA/SIS connected to a pump. (d) Comparison of crude oil extraction processes under 0 kW·m^{-2} and 1 kW·m^{-2}. (e) The process of recovering crude oil from CB@AUA/SIS. (f) Adsorption and recovery capacity of CB@AUA/SIS for crude oil during 10 cyclic tests.

where k is the diffusion rate constant, and C represents the boundary layer effect. This model enables the identification of multiple diffusion stages during adsorption. In the absence of light, the diffusion curve exhibited no clear multilinear features, indicating that internal diffusion was not effectively activated (Figure 4f). But under 1 kW·m^{-2} irradiation, the model revealed a clear three-stage adsorption behavior characterized by an initial rapid surface adsorption, a subsequent diffusion-dominated stage, and a final equilibrium stage. These results demonstrate that light irradiation accelerates surface adsorption and promotes oil diffusion within the composite, thereby enhancing overall adsorption.[18] This enhancement is supported by the membrane's structural characteristics. The large internal pore area (14.882 m^2/g) provides abundant interfaces that facilitate oil capture, while the 10−100 μm pore network allows for rapid oil infiltration once its viscosity is reduced by the photothermal effect (Figure S1). The oil droplet adsorption experiments provided direct visual evidence for these findings (Figure 4g). Without irradiation, the crude oil remained almost unchanged even after 10 min, whereas it was rapidly adsorbed within 1 min under 1 kW·m^{-2}. The sample without CB filler exhibited poor adsorption even under irradiation, confirming that the photothermal effect endowed by CB is essential for achieving efficient oil adsorption (Figures S8 and S9).[44] The CB@AUA/SIS membrane exhibits a relatively high adsorption performance compared to most reported adsorbents, even if the crude oil viscosity used is far greater than most of them (Table S1).

Practical Application of CB@AUA/SIS Membrane

The practical applicability of the CB@AUA/SIS membrane was demonstrated through light-driven crude oil adsorption and recovery. Upon light irradiation, the CB@AUA/SIS membrane could efficiently clean oil-contaminated water surfaces, while its adsorption capacity was significantly lower in the dark (Figure 5a). In addition to the enhanced uptake, the CB@AUA/SIS membrane exhibited excellent oil−water selectivity, with negligible water uptake and high oil adsorption under light conditions (Figure 5b). This performance is attributed to its hydrophobic surface, which shows a water contact angle of 126.5° (Figure S10). For the recycling of the membrane and the adsorbed oil, the oil-containing membrane

https://doi.org/10.1021/acsami.6c03950
ACS Appl. Mater. Interfaces XXXX, XXX, XXX−XXX

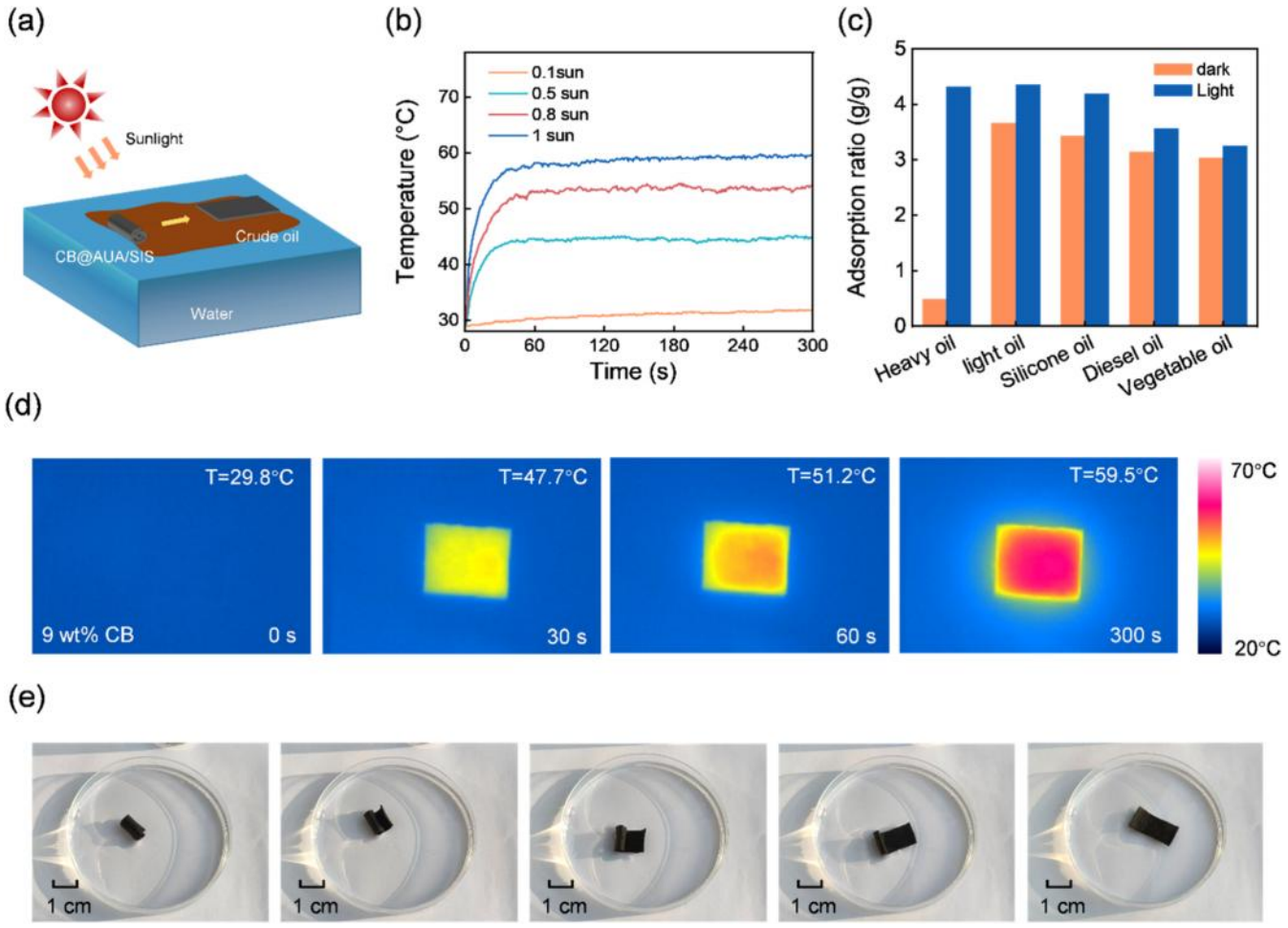

Figure 6. The performance of CB@AUA/SIS under sunlight. (a) The schematic of oil adsorption by CB@AUA/SIS under sunlight. (b) Temperature−time curves of CB@AUA/SIS under different outdoor light intensities. (c) The adsorption capacity of the CB@AUA/SIS for different oil solvents. (d) The thermal images of CB@AUA/SIS during the heating process. (e) Photograph of the membrane's shape recovery process on the water surface under the sun.

could be connected to a pump, and the adsorbed oil could be extracted under light irradiation (Figure 5c), as photothermal heating lowered the crude oil viscosity for effective pumping, while the pump failed under dark conditions (Figure 5d). The crude oil adsorbed by the membrane was efficiently released under light irradiation, enabling effective recovery (Figure 5e). Moreover, the membrane maintained its adsorption capacity over multiple cycles, demonstrating excellent stability and reusability for practical applications (Figure 5f). The CB@AUA/SIS membrane also exhibits a light-responsive shape memory effect that remains effective on the water surface. Under illumination, the deformed membrane gradually recovered to its original shape to maximize the contact area for efficient oil adsorption (Movie S2). A similar response was observed in crude oil (Figure S11), where the membrane unfolded upon irradiation and effectively adsorbed oil, confirming that the light-responsive shape recovery remains functional under practical operating conditions. The autonomous unfolding progressively expands the contact area between the membrane and crude oil. This process elevates the adsorption capacity to 1.12 g·cm^{-3}, compared to 0.33 g·cm^{-3} for a membrane restricted to a fixed geometry. This finding demonstrates the crucial role of shape-memory behavior in providing a compact form for convenient portability and efficient oil recovery upon deployment.

The Performance of CB@AUA/SIS Membrane Under Sunlight Illumination

The CB@AUA/SIS membrane exhibits strong outdoor applicability for crude oil recovery from water surfaces, achieved through its sunlight-responsive shape memory behavior and efficient photothermal adsorption capability (Figure 6a). The membrane exhibited rapid photothermal heating and reached 59.5 °C at 1 sun irradiation, which is consistent with the efficiency previously observed under simulated solar light (Figure 6b). The photothermal effect enhanced the adsorption of various crude oils under sunlight compared to dark conditions (Figure 6c). This efficient heating was visually evidenced by the temperature rise of CB@AUA/SIS in outdoor infrared thermal images (Figure 6d), whereas the AUA/SIS showed negligible heating (Figure S12), confirming the essential role of CB in enabling effective solar-driven oil uptake. The photothermal stability of the membrane was confirmed by repeated heating−cooling cycles under sunlight (Figure S13), highlighting the reusability of the membrane. In a practical outdoor scenario, a prefolded CB@AUA/SIS membrane gradually recovered its original shape under sunlight, expanding its contact area and improving oil

https://doi.org/10.1021/acsami.6c03950
ACS Appl. Mater. Interfaces XXXX, XXX, XXX−XXX

adsorption from the water surface (Figure 6e). This shape memory capability allows the material to be compactly stored and transported, and to deploy its adsorption function under sunlight, demonstrating the practical potential for light-driven oil recovery from water surfaces.

CONCLUSION

In summary, we successfully developed a light-responsive CB@AUA/SIS membrane that integrates photothermal conversion, shape memory recovery, and high lipophilicity. The incorporation of CB endowed the membrane with strong broadband light absorption of up to 98% and a high photothermal conversion efficiency of 73.4%. This performance enabled the membrane to be heated rapidly to 61.2 °C under 1 kW·m^{-2} illumination. This temperature rise effectively reduced the viscosity of highly viscous crude oil (1.8×10^5 mPa·s at room temperature), leading to an impressive adsorption rate of 6240 g·m^{-2}·min^{-1}. The membrane also exhibited excellent oil−water selectivity and maintained reliable performance over multiple adsorption−recovery cycles. Beyond these photothermal benefits, the CB@AUA/SIS exhibited a robust light-responsive shape memory effect. It could be folded for convenient storage and transport, and autonomously unfolded on the water surface under sunlight to restore its full contact area without loss of adsorption capacity. Outdoor sunlight experiments confirmed that CB@AUA/SIS maintained the consistent photothermal heating performance and efficient adsorption of viscous crude oil on water surfaces in practical scenarios. This combination of photothermal response and shape recovery enabled the CB@AUA/SIS membrane to efficiently adsorb highly viscous crude oil under sunlight, maintaining convenient portability and highlighting its potential as a cost-effective and sustainable adsorbent for practical oil spill remediation.

EXPERIMENTAL SECTION

Materials

AUA (65−85 Pa·s at 25 °C) was provided by Shanghai Titan Technology Co., Ltd. SIS (Polystyrene ≥ 22 wt %) was obtained from Guangzhou Rentai Technology Co., Ltd. 2,4,6-trimethylbenzoyldiphenyl phosphine oxide (TPO) was provided by Shanghai Aladdin Biochemical Technology Co., Ltd. Carbon black (CB, diameter = 30−45 nm) were purchased from Nanjing XFNANO Materials Tech Co., Ltd. Trichloromethane ($CHCl_3$, purity ≥ 99%) was obtained from Shenzhen Huashi Technology Co., Ltd. N, N-Dimethylformamide (DMF, purity ≥ 99.9%) was obtained from Guangzhou ChemMole Biotechnology Co., Ltd. Deionized water was used in all experiments. All the chemicals were of analytical grade and used without further purification.

Preparation of the Solution

AUA (1 g) and SIS (2 g) with a concentration of 25 wt % were dissolved in $CHCl_3$/DMF solvent with a weight ratio of 9:1. A 2 wt % concentration of TPO (0.06 g) was added to the solution as an initiator. This mixture was thoroughly stirred in the dark for 12 h to ensure homogeneity. For the doping of the composite SMP, CB was incorporated into the aforementioned homogeneous solution. The solution underwent sonication at a power level of 100 W for 30 min, and then was stirred at 400 rpm for 5 h.

Fabrication of Shape Memory Oil-Adsorbing Fibers

Fibers were fabricated from the mixed solution via electrospinning using a configured system. The fibers were electrospun at an applied voltage of 20 kV for all solutions at a tip-to-collector distance of 15 cm. The feed rate was maintained at 1.3 mL/h for the solution. A ultraviolet curing lamp (wavelength: 295 nm) was mounted 5 cm above the sample receiving plate. The fibers were then irradiated continuously under this fixed light source to achieve complete curing. The fibers were used as adsorbents with no further treatment.

Morphology and Composition Test

The surface morphology of electrospun fibers was observed by field emission scanning electron microscopy (MIRA3, TESCAN) with an accelerating voltage of 10 kV, and transmission electron microscopy (Talos F200X, ThermoFisher Scientific) with a working voltage of 200 kV.

EDS analysis was performed with an Oxford Instruments X-MaxN EDS detector coupled to a scanning electron microscope (SEM), using the analysis software Aztec 3.1 from Oxford Instruments.

The pore size distribution and pore volume were determined by mercury intrusion porosimetry (Autopore V 9600, Micromeritics) with a measurement range of 5.5 nm-340 μm.

Thermodynamic Performance Test

Tension experiments were conducted on specimens with a gauge length of 20 mm and a cross-section of 5 mm × 1 mm using a microcomputer-controlled electronic universal testing machine (LE3153, Lishi) at a tensile rate of 0.3 mm/s.

The thermal stability of the material is tested by the thermal analysis system (TGA/DSC 1, METTLER TOLEDO). The samples were heated from 30 to 600 °C at a heating rate of 5 °C/min under nitrogen vapor.

The damping properties were evaluated using a dynamic mechanical analyzer (DMA242E, NETZSCH). Samples with dimensions of 20 × 5 × 1 mm^3 were tested at a frequency of 1 Hz and an amplitude of 10 μm. The temperature was first equilibrated at 0 °C for 5 min and then gradually increased to 200 °C at a heating rate of 5 °C/min.

The thermal conductivity of the samples was measured using a laser flash apparatus (LFA 467 HyperFlash, NETZSCH). The samples, with a diameter of 12.7 mm, were subjected to the test to determine their thermal conductivity properties.

The shape memory properties of the AUA/SIS and CB@AUA/SIS were evaluated using a dynamic mechanical analyzer (Q850 DMA, TA Instruments). To characterize the shape memory properties, the sample was initially heated to 90 °C and subjected to a compressive strain (ε_1). It was then cooled to 25 °C, allowing the stress to be released, resulting in a fixity strain (ε_2). The sample was subsequently reheated to 90 °C, and the compressive strain was restored to ε_3. The shape fixity ratio (R_f) and the shape recovery ratio (R_r) were calculated using eq 3 and eq 4, respectively:

$$R_f = \frac{\varepsilon_2}{\varepsilon_1} \times 100\% \tag{3}$$

$$R_r = \frac{\varepsilon_1 - \varepsilon_3}{\varepsilon_1} \times 100\% \tag{4}$$

Photothermal Performance Test

The UV−vis absorption spectra were measured in air using the UV−vis spectroscopy (HITACHI, UH5700) with a wavelength range of 250−2500 nm.

The surface temperature distribution and thermal response characteristics of the material under light irradiation were characterized using an infrared thermography system (X640F150MF25, YOSEEN INFRARED).

Calculation of Photothermal Conversion Efficiency

The photothermal conversion efficiency (PCE) of CB@AUA/SIS membranes was evaluated under simulated solar irradiation (AM 1.5 G, 1 sun). The membranes were irradiated, and the temperature rise was recorded in real-time using an infrared thermal imaging camera until thermal equilibrium was reached.

After switching off the light source, the cooling process was monitored to obtain the heat transfer coefficient. The dimensionless temperature parameter θ was defined according to eq 5

https://doi.org/10.1021/acsami.6c03950
ACS Appl. Mater. Interfaces XXXX, XXX, XXX−XXX

$$\theta = \frac{T_t - T_{surr}}{T_{max} - T_{surr}} \quad (5)$$

where T_t is the instantaneous temperature, T_{max} is the equilibrium temperature under irradiation, and T_{surr} is the ambient temperature. The cooling process follows an exponential decay as expressed in eq 6

$$\theta = e^{-t/\tau_s} \quad (6)$$

where τ_s is the system time constant. By plotting -ln(θ) versus time, the slope of the linear fit yields $1/\tau_s$.

The heat transfer coefficient was then obtained from eq 7

$$\tau_s = \frac{m_d C_d}{hS} \quad (7)$$

where m_d and C_d are the mass and heat capacity of the system, respectively. C_d was determined using differential scanning calorimetry (DSC) via the standard sapphire method.

The absorbed solar power was calculated using eq 8 by integrating the standard AM 1.5G (1 kW·m^{-2}) solar spectrum weighted by the wavelength-dependent absorbance of the membrane

$$P_{in} = \bar{\alpha}(\lambda) \int_{300}^{2500} I(\lambda) d\lambda \quad (8)$$

where $I(\lambda)$ is the spectral irradiance of the standard AM 1.5G solar spectrum, and in the actual calculations, $\bar{\alpha}(\lambda)$ is taken as the average absorbance of the material within this wavelength range.

The photothermal conversion efficiency (η) was determined using eq 9

$$\eta = \frac{hS(T_{max} - T_{surr})}{P_{in}} \quad (9)$$

Oil Adsorption Performance Test

The viscosity of crude oil was measured using a rotational rheometer (HAAKE MARS 40, Thermo Fisher Scientific, Germany) with a parallel-plate geometry. Temperature-dependent viscosity measurements were performed over the range of 15 to 95 °C with a heating rate of 2 °C/min. The tests were conducted in oscillatory mode under strain control (1%) at an angular frequency of 10 s^{-1}.

The contact angle measurements were performed using Attension Theta Flex from Biolin Scientific. Approximately 9 μL of liquid was dispensed for each measurement.

The oil adsorption rate under different light intensities was determined after irradiation of the membrane for a preset duration. The irradiated membrane was immediately placed on the surface of the crude oil and then promptly removed. The adsorbed oil mass (m) was measured, and the adsorption rate was calculated as $\frac{m}{S \times t}$, where S is the contact area and t is the contact time.

The oil adsorption capacity (Q_m) was measured by immersing the membrane in crude oil until saturation. The membrane was weighed before (m_1) and after (m_t) adsorption, and the capacity was calculated using $\frac{m_t - m_1}{m_1}$.

ASSOCIATED CONTENT

Supporting Information

The Supporting Information is available free of charge at https://pubs.acs.org/doi/10.1021/acsami.6c03950.

Shape recovery process of CB@AUA/SIS in response to light (MP4)

Light-responsive shape recovery and oil adsorption of CB@AUA/SIS on water surface (MP4)

Additional figures and a table including pore characteristics; EDS spectra, SEM images, storage modulus, temperature−time heating and cooling curves, thermal images, crude oil adsorption performance and rates, contact angles, shape recovery photographs; and a performance comparison with other works (PDF)

AUTHOR INFORMATION

Corresponding Authors

Lingyu Zhao − *Department of Materials Science and Engineering, Southern University of Science and Technology, Shenzhen 518055, China*; Email: zhaoly@sustech.edu.cn

Jinsong Leng − *Center for Composite Materials and Structures, Harbin Institute of Technology, Harbin 150080, China*; orcid.org/0000-0001-5098-9871; Email: lengjs@hit.edu.cn

Authors

Qiong Zuo − *Department of Materials Science and Engineering, Southern University of Science and Technology, Shenzhen 518055, China*

Qingyuan Du − *Department of Materials Science and Engineering, Southern University of Science and Technology, Shenzhen 518055, China*

Zengbai Ouyang − *Department of Materials Science and Engineering, Southern University of Science and Technology, Shenzhen 518055, China*

Yutong Wang − *Department of Materials Science and Engineering, Southern University of Science and Technology, Shenzhen 518055, China*

Dazhi Sun − *Department of Materials Science and Engineering, Southern University of Science and Technology, Shenzhen 518055, China*; orcid.org/0000-0001-7553-3141

Complete contact information is available at: https://pubs.acs.org/10.1021/acsami.6c03950

Author Contributions

§Q.Z. and L.Z. contributed equally to this work. The manuscript was written through contributions of all authors. All authors have given approval to the final version of the manuscript.

Notes

The authors declare no competing financial interest.

ACKNOWLEDGMENTS

The work was funded by the Basic Research Program of Shenzhen (JCYJ20230807093559046), National Natural Science Foundation of China (92471203).

REFERENCES

(1) Yang, C.; Long, M.; Ding, C.; Zhang, R.; Zhang, S.; Yuan, J.; Zhi, K.; Yin, Z.; Zheng, Y.; Liu, Y.; Wu, H.; Jiang, Z. Antifouling Graphene Oxide Membranes for Oil-Water Separation via Hydrophobic Chain Engineering. *Nat. Commun.* **2022**, *13*, No. 7334.

(2) Wang, Z.; An, C.; Lee, K.; Owens, E.; Chen, Z.; Boufadel, M.; Taylor, E.; Feng, Q. Factors Influencing the Fate of Oil Spilled on Shorelines: A Review. *Environ. Chem. Lett.* **2021**, *19*, 1611−1628.

(3) Escobar, H. Mystery Oil Spill Threatens Marine Sanctuary in Brazil. *Science* **2019**, *366*, No. 672.

(4) Brussaard, C. P. D.; Peperzak, L.; Beggah, S.; Wick, L. Y.; Wuerz, B.; Weber, J.; Samuel Arey, J.; Van Der Burg, B.; Jonas, A.; Huisman, J.; Van Der Meer, J. R. Immediate Ecotoxicological Effects of Short-Lived Oil Spills on Marine Biota. *Nat. Commun.* **2016**, *7*, No. 11206.

(5) Barron, M. G.; Vivian, D. N.; Heintz, R. A.; Yim, U. H. Long-Term Ecological Impacts from Oil Spills: Comparison of Exxon

https://doi.org/10.1021/acsami.6c03950
ACS Appl. Mater. Interfaces XXXX, XXX, XXX−XXX

Valdez, Hebei Spirit, and Deepwater Horizon. *Environ. Sci. Technol.* **2020**, *54*, 6456−6467.
(6) Cheng, X.; Ye, Y.; Li, Z.; Chen, X.; Bai, Q.; Wang, K.; Zhang, Y.; Drioli, E.; Ma, J. Constructing Environmental-Friendly "Oil-Diode" Janus Membrane for Oil/Water Separation. *ACS Nano* **2022**, *16*, 4684−4692.
(7) Yuan, D.; Zhang, T.; Guo, Q.; Qiu, F.; Yang, D.; Ou, Z. A Novel Hierarchical Hollow SiO2@MnO2 Cubes Reinforced Elastic Polyurethane Foam for the Highly Efficient Removal of Oil from Water. *Chem. Eng. J.* **2017**, *327*, 539−547.
(8) Sui, S.; Quan, H.; Yang, X.; Dong, X.; Ji, Y.; Liu, C.; Xu, G.; Guo, S.; Zhang, Y. Multifunctional Modified Polyurethane Sponge for Recovery of Oil Spills and Photocatalytic Degradation. *Compos. Part B-Eng.* **2024**, *271*, No. 111176.
(9) Guan, H.; Lian, R.; Li, R.; Zhu, J.; Zhao, Z.; Liu, L.; Chen, X.; Jiao, C.; Kuang, S. A Low-Temperature Carbonization Strategy for Efficient Viscous Crude Oil Spill Disposal without Hydrophobic Coating: CoFe-PBA-Catalyzed Carbonization of Superhydrophobic Flame Retardant Melamine Sponge. *Adv. Funct. Mater.* **2024**, *34*, No. 2313224.
(10) Qi, X.; Li, C.; Zou, X.; He, L.; Liu, Z.; Gao, Z. Super-Hydrophobic Graphene-Based High Elastic Sponge with Superior Photothermal Effect for Efficient Cleaning of Oil Contamination. *Chem. Eng. J.* **2023**, *476*, No. 146317.
(11) Song, P.; Cui, J.; Di, J.; Liu, D.; Xu, M.; Tang, B.; Zeng, Q.; Xiong, J.; Wang, C.; He, Q.; Kang, L.; Zhou, J.; Duan, R.; Chen, B.; Guo, S.; Liu, F.; Shen, J.; Liu, Z. Carbon Microtube Aerogel Derived from Kapok Fiber: An Efficient and Recyclable Sorbent for Oils and Organic Solvents. *ACS Nano* **2020**, *14*, 595−602.
(12) Guan, H.; Cheng, Z.; Wang, X. Highly Compressible Wood Sponges with a Spring-like Lamellar Structure as Effective and Reusable Oil Absorbents. *ACS Nano* **2018**, *12*, 10365−10373.
(13) Wong, T. W.; Wu, J.; Yang, M.; Abdul Kadir, M. R.; Wahit, M. U.; Zhao, Q. Multifunctional Shape-Memory Foams with Highly Tunable Properties via Organo-Phase Cryo-Polymerization. *J. Mater. Chem. A* **2017**, *5*, 9793−9800.
(14) Lee, S.; Lee, G.; Ryu, J.; Lee, D. W. Surfactant-Free, Spray-Assisted Water Droplet Templating for Efficient Fabrication of Ultraviolet-Curable Polydimethylsiloxane Sponge as a Reusable Oil Cleanup Sorbent. *Chem. Eng. J.* **2024**, *488*, No. 150958.
(15) Chu, Z.; Feng, Y.; Xu, T.; Zhu, C.; Li, K.; Li, Y.; Yang, Y.; Yang, Z. Magnetic, Self−Heating and Superhydrophobic Sponge for Solar−Driven High−Viscosity Oil−Water Separation. *J. Hazard. Mater.* **2023**, *445*, No. 130553.
(16) Kuang, Y.; Chen, C.; Chen, G.; Pei, Y.; Pastel, G.; Jia, C.; Song, J.; Mi, R.; Yang, B.; Das, S.; Hu, L. Bioinspired Solar-Heated Carbon Absorbent for Efficient Cleanup of Highly Viscous Crude Oil. *Adv. Funct. Mater.* **2019**, *29*, No. 1900162.
(17) Ku, B. J.; Lee, B. M.; Kim, D. H.; Mnoyan, A.; Hong, S. K.; Go, K. S.; Kwon, E. H.; Kim, S. H.; Choi, J. H.; Lee, K. Photothermal Fabrics for Efficient Oil-Spill Remediation via Solar-Driven Evaporation Combined with Adsorption. *ACS Appl. Mater. Interfaces.* **2021**, *13*, 13106−13113.
(18) Sun, A.; Hou, X.; Hu, X. Super-Performance Photothermal Conversion of 3D Macrostructure Graphene-CuFeSe2 Aerogel Contributes to Durable and Fast Clean-up of Highly Viscous Crude Oil in Seawater. *Nano Energy* **2020**, *70*, No. 104511.
(19) Qi, X.; Wu, J.; He, L.; Wei, W.; Wang, J.; Chen, S.; Li, J.; Gao, Z. Silane Grafted Graphene Superhydrophobic Coating Coated Non-Woven Fabric for Photothermal Driven High Viscosity Oil-Water Separation. *Carbon* **2025**, *233*, No. 119886.
(20) Gong, F.; Li, H.; Yuan, X.; Huang, J.; Xia, D.; Papavassiliou, D. V.; Xiao, R.; Yamauchi, Y.; Wu, K. C. W.; Ok, Y. S. Recycling Polymeric Solid Wastes for Energy-Efficient Water Purification, Organic Distillation, and Oil Spill Cleanup. *Small* **2021**, *17*, No. 2102459.
(21) Lian, Y.; Wang, X.; Chen, H.; Hu, Y.; Liang, M.; Huang, Q.; Chen, Z.; Liu, Y.; Zhang, Y. Photothermal Superhydrophobic LA-MOF@PDA@MS Sponge for Offshore Crude Oil Recovery. *Compos. Part B-Eng.* **2026**, *308*, No. 113012.
(22) Lu, Y.; Chen, Z.; Wei, M.; Li, Z.; Gao, C.; Qin, L.; Xue, L. Smart Methylcellulose-Based Foams with Thermal-Induced Volume Shrinkage for Efficient Oil Absorption and Controllable Recovery. *Carbohydr. Polym.* **2025**, *370*, No. 124397.
(23) Lu, H.; Lu, Y.; Ling, Z.; Du, J.; Qiu, J. A Novel Approach to Marine Oil Spill Response: A Solar-Powered Light-Heat-Electricity Absorption System. *Chem. Eng. J.* **2025**, *505*, No. 159192.
(24) Liu, Z.; Wu, F.; Lv, T.; Qu, Y.; Zhang, Z.; Yu, C.; Zhao, C.; Xing, G. Ti3C2TX/Carbon Aerogels Derived from Winter Melon for High-Efficiency Photothermal Conversion. *Desalination* **2024**, *573*, No. 117207.
(25) Bhardwaj, N.; Bhaskarwar, A. N. A Review on Sorbent Devices for Oil-Spill Control. *Environ. Pollut.* **2018**, *243*, 1758−1771.
(26) Gu, J.; Ji, L.; Xiao, P.; Zhang, C.; Li, J.; Yan, L.; Chen, T. Recent Progress in Superhydrophilic Carbon-Based Composite Membranes for Oil/Water Emulsion Separation. *ACS Appl. Mater. Interfaces* **2021**, *13*, 36679−36696.
(27) Guo, M.; Guo, J.; Jia, D.; Zhao, H.; Sun, Z.; Song, X.; Li, Y. Coal Derived Porous Carbon Fibers with Tunable Internal Channels for Flexible Electrodes and Organic Matter Absorption. *J. Mater. Chem. A* **2015**, *3*, 21178−21184.
(28) Byun, S.; Park, S.; Lee, E. J.; An, A. K.; Jeong, S. Joule-Heating Electrospun Reduced-Graphene Oxide Nanoribbon-Coated Reusable Polymeric Sorbent with an Excellent Sorption/Desorption of High-Viscosity Oils. *Carbon* **2024**, *219*, No. 118826.
(29) Holmberg, S.; Garza-Flores, N. A.; Almajhadi, M. A.; Chávez-Madero, C.; Lujambio-Angeles, A.; Jind, B.; Bautista-Flores, C.; Mendoza-Buenrostro, C.; Pérez-Carrillo, E.; Wickramasinghe, H. K.; Martínez-Chapa, S. O.; Madou, M.; Weiss, P. S.; Álvarez, M. M.; Trujillo-de Santiago, G. Fabrication of Multilayered Composite Nanofibers Using Continuous Chaotic Printing and Electrospinning: Chaotic Electrospinning. *ACS Appl. Mater. Interfaces* **2021**, *13*, 37455−37465.
(30) Obaid, M.; Tolba, G. M. K.; Motlak, M.; Fadali, O. A.; Khalil, K. A.; Almajid, A. A.; Kim, B.; Barakat, N. A. M. Effective Polysulfone-Amorphous SiO2 NPs Electrospun Nanofiber Membrane for High Flux Oil/Water Separation. *Chem. Eng. J.* **2015**, *279*, 631−638.
(31) Guo, H.; Puttreddy, R.; Salminen, T.; Lends, A.; Jaudzems, K.; Zeng, H.; Priimagi, A. Halogen-Bonded Shape Memory Polymers. *Nat. Commun.* **2022**, *13*, No. 7436.
(32) Wang, L.; Zhang, F.; Liu, Y.; Leng, J. Shape Memory Polymer Fibers: Materials, Structures, and Applications. *Adv. Fiber Mater.* **2022**, *4*, 5−23.
(33) Ni, R.; Zhang, L.; Ma, J.; Zhang, J.; Xu, X.; Shi, H.; Deng, Q.; Hu, W.; Hu, J.; Ke, Q.; Zhao, Y. Versatile Keratin Fibrous Adsorbents with Rapid-Response Shape-Memory Features for Sustainable Water Remediation. *Nano Lett.* **2024**, *24*, 12891−12899.
(34) Zhao, L.; Wang, L.; Shi, J.; Hou, X.; Wang, Q.; Zhang, Y.; Wang, Y.; Bai, N.; Yang, J.; Zhang, J.; Yu, B.; Guo, C. F. Shape-Programmable Interfacial Solar Evaporator with Salt-Precipitation Monitoring Function. *ACS Nano* **2021**, *15*, 5752−5761.
(35) Zhang, W.; Zou, C.; Pan, Q.; Hu, G.; Shi, H.; Zhang, Y.; He, X.; He, Y.; Zhang, X. A Triple Shape Memory Material of Trans-Polyisoprene/Polycaprolactone with Customizable Response Temperature Controlled by Crosslinking Density. *Adv. Funct. Mater.* **2024**, *34*, No. 2400245.
(36) Guo, Y.; Li, C.; Wei, P.; Hou, K.; Zhu, M. Scalable Carbon Black Deposited Fabric/Hydrogel Composites for Affordable Solar-Driven Water Purification. *J. Mater. Sci. Technol.* **2022**, *106*, 10−18.
(37) Oh, S.; Bang, J.; Jin, H. J.; Kwak, H. W. Green Fabrication of Underwater Superoleophobic Biopolymeric Nanofibrous Membranes for Effective Oil−Water Separation. *Adv. Fiber Mater.* **2023**, *5*, 603−616.
(38) Zhang, H.; Zhang, G.; Tang, M.; Zhou, L.; Li, J.; Fan, X.; Shi, X.; Qin, J. Synergistic Effect of Carbon Nanotube and Graphene Nanoplates on the Mechanical, Electrical and Electromagnetic

https://doi.org/10.1021/acsami.6c03950
ACS Appl. Mater. Interfaces XXXX, XXX, XXX−XXX

Interference Shielding Properties of Polymer Composites and Polymer Composite Foams. *Chem. Eng. J.* **2018**, *353*, 381−393.
(39) Zhang, W.; Deng, X.; Sui, G.; Yang, X. Improving Interfacial and Mechanical Properties of Carbon Nanotube-Sized Carbon Fiber/Epoxy Composites. *Carbon* **2019**, *145*, 629−639.
(40) Dorigato, A.; Pegoretti, A. Shape Memory Epoxy Nanocomposites with Carbonaceous Fillers and In-Situ Generated Silver Nanoparticles. *Polym. Eng. Sci.* **2019**, *59*, 694−703.
(41) Guo, B.; Feng, G.; Manghnani, P. N.; Cai, X.; Liu, J.; Wu, W.; Xu, S.; Cheng, X.; Teh, C.; Liu, B. A Porphyrin-Based Conjugated Polymer for Highly Efficient In Vitro and In Vivo Photothermal Therapy. *Small* **2016**, *12*, 6243−6254.
(42) Li, T. T.; Wang, Z.; Ren, H. T.; Peng, H. K.; Zhang, X.; Jiang, Q.; Lou, C. W.; Lin, J. H. Recyclable and Degradable Nonwoven-Based Double-Network Composite Hydrogel Adsorbent for Efficient Removal of Pb(II) and Ni(II) from Aqueous Solution. *Sci. Total Environ.* **2021**, *758*, No. 143640.
(43) Wang, Z.; Barford, J. P.; Hui, C. W.; McKay, G. Kinetic and Equilibrium Studies of Hydrophilic and Hydrophobic Rice Husk Cellulosic Fibers Used as Oil Spill Sorbents. *Chem. Eng. J.* **2015**, *281*, 961−969.
(44) Li, R.; Geng, Y.; Wei, S.; Zhao, Z.; Zhang, H.; Chen, X.; Jiao, C.; Kuang, S. Magnetic, Self-Heating and Superhydrophobic Sponge Decorated with BN and CoFe2O4 for High-Efficient Cleanup of Crude Oil Spills Using Facile Co-Precipitation Strategy. *Sep. Purif. Technol.* **2025**, *354*, No. 128952.

https://doi.org/10.1021/acsami.6c03950
ACS Appl. Mater. Interfaces XXXX, XXX, XXX−XXX